J. Fluid Mech. (1996), *vol.* 329, *pp.* 65–88

Natural convection in an enclosure having a vertical sidewall with time-varying temperature

By HO SANG KWAK[1] AND JAE MIN HYUN[2]†

[1] Space Environment Laboratory, Institute of Space and Astronautical Science, 3-1-1 Yoshinodai, Sagamihara, Kanagawa 229, Japan

[2] Department of Mechanical Engineering, Korea Advanced Institute of Science and Technology, 373-1, Kusong-dong, Yusong-gu, Taejon 305-701, South Korea

(Received 18 September 1995 and in revised form 10 June 1996)

A numerical study is performed for time-varying natural convection of an incompressible Boussinesq fluid in a sidewall-heated square cavity. The temperature at the cold sidewall T_C is constant, but at the hot sidewall a time-varying temperature condition is prescribed, $T_H = \overline{T_H} + \Delta T' \sin ft$. Comprehensive numerical solutions are found for the time-dependent Navier–Stokes equations. The numerical results are analysed in detail to show the existence of resonance, which is characterized by maximal amplification of the fluctuations of heat transfer in the interior. Plots of the dependence of the amplification of heat transfer fluctuations on the non-dimensional forcing frequency ω are presented. The failure of Kazmierczak & Chinoda (1992) to identify resonance is shown to be attributable to the limitations of the parameter values they used. The present results illustrate that resonance becomes more distinctive for large Ra and $Pr \sim O(1)$. The physical mechanism of resonance is delineated by examining the evolution of oscillating components of flow and temperature fields. Specific comparisons are conducted for the resonance frequency ω_r between the present results and several other previous predictions based on the scaling arguments.

1. Introduction

Natural convection in a closed cavity with different temperatures imposed on the two facing vertical sidewalls has been extensively studied in recent years (e.g. Ostrach 1982; Hyun 1994). For a geometrically simple rectangular enclosure, the major non-dimensional parameters are the Rayleigh number $Ra \equiv \alpha g \Delta T H^3/\nu\kappa$, the cavity aspect ratio $A \equiv H/L$, and the Prandtl number $Pr \equiv \nu/\kappa$. In the above, g denotes the acceleration due to gravity, α the coefficient of thermometric expansion, ΔT the temperature difference between the two vertical walls, ν the kinematic viscosity, κ the thermal diffusivity, and H and L the height and width of the enclosure, respectively. Interest is often focused in the convection-dominant regime $Ra \gg 1$. For a standard configuration $A = 1$, benchmark solutions have been published to describe the flow and thermal fields (de vahl Davies & Jones 1983).

Most of the studies on natural convection in an enclosure have dealt with situations when the boundary conditions are enforced in a time-invariant manner (Ostrach 1982). Convection in a confined space, driven by time-dependent boundary conditions, constitutes a separate class of problems. A classical flow configuration was proposed by Patterson & Imberger (1980). In this model, the fluid and the rectangular container surfaces are motionless and in thermal equilibrium at uniform temperature T_0 at the

† To whom correspondence should be addressed.

initial state. At time $t = 0$, the temperatures at the two vertical surfaces are abruptly changed to $T_0 + \frac{1}{2}\Delta T$ and $T_0 - \frac{1}{2}\Delta T$, respectively. The horizontal surfaces are insulated. The subsequent evolution of flow and thermal fields inside the enclosure, in response to this step change in the boundary conditions, was depicted. Various essential transient characteristics pertinent to this basic model have been explored by numerous investigators (e.g. Yewell, Poulikakos & Bejan 1982; Ivey 1984; Paolucci & Chenoweth 1989; Le Quéré 1990; Paolucci 1990; Patterson & Armfield 1990; Bark, Alavyoon & Dahlkild 1992).

As observed by Lage & Bejan (1993) and Hyun (1994), accounts of unsteady natural convection in an enclosure, in which the thermal boundary conditions undergo continuous temporal variations, are scarce. Vasseur & Robillard (1982) considered convective cooling of a fluid in a cavity with a sidewall of temporally decreasing temperature. Schladow, Patterson & Street (1989) treated natural convection in a cavity, in which the temperatures of the wall increased linearly with time. The primary intention of these works was to verify certain numerical techniques or to explain the discrepancies between numerical simulations and experimental results. The rudimentary physics was basically similar to the unsteady convection due to a step change in thermal conditions in the sidewall-heated cavity.

A significantly new approach was taken by Lage & Bejan (1993). Instead of the usual step change in thermal boundary conditions, they considered cases when the thermal boundary conditions were continuously changing with time. Specifically, interest was directed at a rectangular cavity with a constant-temperature cold sidewall. At the other vertical sidewall, a time-dependent heat flux was prescribed. The heat flux fluctuated in a square-wave fashion about the mean value. The fundamental question concerned the way in which the periodicity of the sidewall heating affected the time-dependent flow and attendant heat transfer in the enclosure. The crux of the argument is focused on the possibility of 'resonance' of the fluid system with the oscillation of the externally supplied heat input at the vertical sidewall.

Physically, resonance describes the phenomenon that the eigenmodes of a system are excited and amplified if this system is exposed to an external excitation with the correct natural frequency. This problem statement has serious ramifications from the standpoint of the fundamental dynamics of natural convection. In practical applications, the problem models, for example, natural convection in a room which is heated periodically on a daily basis. Even more appealing is the convection in a confined space in many electronic devices, where time-dependent flows are induced due to the periodic energizing of the 'on' and 'off' modes.

The numerical studies of Lage & Bejan (1993), at high Rayleigh numbers, clearly established the existence of resonance for periodic heating at the sidewall. The resonance was identified by the occurrence of maximal fluctuations of the local velocity and the Nusselt numbers. Also, the resonance frequency f_r as well as the amplification of the Nusselt number Nu are shown to be dependent on Pr. Subsequent scale analyses by Lage & Bejan showed a fair qualitative agreement between the predicted values and the numerical results for f_r. In summary, the study of Lage & Bejan shows good evidence of the existence of resonance phenomenon in natural convection when a continuously changing thermal boundary condition is adopted.

The presence of resonant convection in an enclosure has also been noted in the context of mixed convection. Iwatsu, Hyun & Kuwahara (1992) examined convective motions of an incompressible fluid in a cavity with an externally imposed temperature difference between the top torsionally oscillating hot lid and the bottom stationary cold endwall. The aim was to explore the enhancement of heat transfer in the vertical

direction by means of a mechanically driven oscillation of the top lid. Clearly, if no mechanical oscillation is present, the heat transfer will be entirely conductive in a stably stratified motionless fluid. The results of extensive numerical computations revealed the existence of resonance for particular frequencies of the lid oscillation. When resonance occurs, heat transfers as well as velocity fluctuations are augmented, which suggest potentially useful applications in technological systems.

In a related problem set-up, Kazmierczak & Chinoda (1992) conducted numerical studies of natural convection in a square cavity with one vertical sidewall at a constant temperature T_C. The temperature at the other vertical sidewall varied sinusoidally in time about the mean value $\overline{T_H}(> T_C)$. The numerical simulations produced periodic solutions for one Rayleigh number ($Ra = 1.4 \times 10^5$) and one Prandtl number ($Pr = 7$) and for three different frequencies of the sidewall temperature oscillations. The solutions demonstrated that the interior flow fluctuations changed monotonically with the frequency of wall temperature oscillations. In essence, no resonance was detected between the temporal variations of the sidewall temperature and the resulting flow oscillations. As to resonance, the numerical account of Kazmierczak & Chinoda (1992) is at variance with the qualitative conclusions of Lage & Bejan (1993) and of Iwatsu *et al.* (1992), although the precise problem formulations may be slightly different.

Flow oscillations in a sidewall-heated cavity have been discussed extensively. Patterson & Imberger (1980) reported the presence of internal gravity oscillation modes in the transient approach to steady state. Ivey (1984) explained the experimentally observed oscillatory transient behaviour based on the concept of internal hydraulic jump. Chenoweth & Paolucci (1986) found that the hydraulic jumps were responsible for the first transition to the time-dependent flow for low aspect ratios. Le Quéré & Alziary de Roquetfort (1986) and Le Quéré (1990) observed the flow oscillations due to the sidewall boundary layer waves. Paolucci & Chenoweth (1989) examined the onset and the frequencies of the oscillatory instabilities. More recently, Xia, Yang & Mukutmoni (1995) investigated the stability of natural convection in a square cavity by using the same problem set-up as Kazmierczak & Chinoda (1992). Attention was given to illustrating the effect of imposed wall temperature oscillations on the onset of oscillatory instability and flow transitions. Only one particular value of the imposed external frequency was considered in their calculations.

Comprehensive and far-ranging numerical computations are performed in the present work for the same problem formulation as was used by Kazmierczak & Chinoda (1992). The purpose is to obtain detailed numerical solutions over a much broader range of the frequency of the hot-wall temperature oscillation. The ranges of relevant parameter values have been considerably extended. By undertaking full-scale numerical calculations and systematic post-processing analyses, a definite assertion will be made as to the existence of the resonance of fluid flows at certain frequencies of the wall temperature oscillations. Furthermore, it will be shown that the previous computational results of Kazmierczak & Chinoda (1992) for three different values of frequency represent only a narrow portion of the whole spectrum of solutions. Owing to the limited frequency resolution achieved by Kazmierczak & Chinoda (1992), distinct evidence of resonance between the flow fluctuation and the frequency of wall temperature oscillation was not found. However, the present numerical results illustrate that the fluctuations of flow and heat transfer responses display peak values at certain frequencies, if computations span much more extended ranges of the frequency with considerably finer resolution. These efforts explain the apparent disagreements among the previous works.

In the present paper, an overview of the time-dependent interior flow and associated

heat transfer, in response to the oscillating sidewall temperature condition, is given. The details of fluctuating flow and temperature fields over a cycle will be thoroughly analysed. Emphasis will be placed on obtaining a physical interpretation of the nature of convective resonance phenomenon. In particular, inspection of the fluctuations of flow and temperature structures, both in the core and in the boundary layers, leads to the identification of the resonance frequency of the system. The numerically obtained resonance frequency is compared with the predictions of the previous models based on scaling arguments. The extensive numerical undertakings of the present study shed light on the fundamental physical mechanism inherent in confined natural convection with time-varying forcing at the boundary.

2. The mathematical formulation

Consider a square cavity (height/width $= H/L = 1.0$), which is filled with an incompressible Boussinesq fluid. All the physical properties are taken to be constant. The top and bottom horizontal walls are thermally insulated. The left-hand vertical wall ($x = 0$) is maintained at a constant temperature T_C. The temperature at the right-hand vertical wall ($x = L$), T_H, varies sinusoidally with time as $T_H = \overline{T_H} + \Delta T' \sin ft$, where the mean value $\overline{T_H} \equiv T_C + \Delta T$, $\Delta T > 0$; $\Delta T'$ and f respectively denote the amplitude and frequency of oscillation. Figure 1 shows a schematic of the flow configuration and coordinate system, and figure 2 depicts the time-varying thermal boundary condition at the hot vertical wall.

The flow is governed by the time-dependent Navier–Stokes equations, which, in non-dimensional form, are

$$\frac{\partial U}{\partial \tau} + \frac{\partial}{\partial X}(U^2) + \frac{\partial}{\partial Y}(VU) = -\frac{\partial P}{\partial X} + \left(\frac{Pr}{Ra}\right)^{1/2} \nabla^2 U, \tag{1}$$

$$\frac{\partial V}{\partial \tau} + \frac{\partial}{\partial X}(UV) + \frac{\partial}{\partial Y}(V^2) = -\frac{\partial P}{\partial Y} + \theta + \left(\frac{Pr}{Ra}\right)^{1/2} \nabla^2 V, \tag{2}$$

$$\frac{\partial \theta}{\partial \tau} + \frac{\partial}{\partial X}(U\theta) + \frac{\partial}{\partial Y}(V\theta) = \left(\frac{1}{Ra\,Pr}\right)^{1/2} \nabla^2 \theta, \tag{3}$$

$$\frac{\partial U}{\partial X} + \frac{\partial V}{\partial Y} = 0, \tag{4}$$

where

$$\nabla^2 = \frac{\partial^2}{\partial X^2} + \frac{\partial^2}{\partial Y^2}.$$

In line with the problem description, the boundary conditions are

$$U = V = \frac{\partial \theta}{\partial Y} = 0 \quad \text{at} \quad Y = 0, 1; \tag{5a}$$

$$U = V = \theta = 0 \quad \text{at} \quad X = 0; \tag{5b}$$

$$U = V = 0, \quad \theta = 1 + \epsilon \sin(\omega \tau) \quad \text{at} \quad X = 1. \tag{5c}$$

In the above, non-dimensionalization has been done in a similar fashion to Lage & Bejan (1991, 1993):

$$\tau = t(Ra\,Pr)^{1/2} \frac{\kappa}{H^2}, \quad (X, Y) = \frac{(x, y)}{H}, \tag{6a, b}$$

$$(U, V) = (u, v)(Ra\,Pr)^{-1/2} \frac{H}{\kappa}, \quad \theta = \frac{T - T_C}{\overline{T_H} - T_C}, \quad P = \frac{(p + \rho g y) H^2}{\rho \kappa^2 Ra\,Pr}. \tag{6c–e}$$

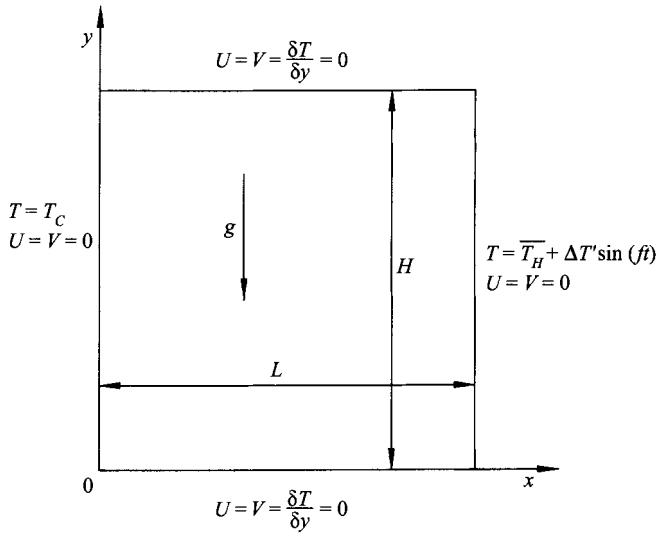

FIGURE 1. Sketch of the flow configuration.

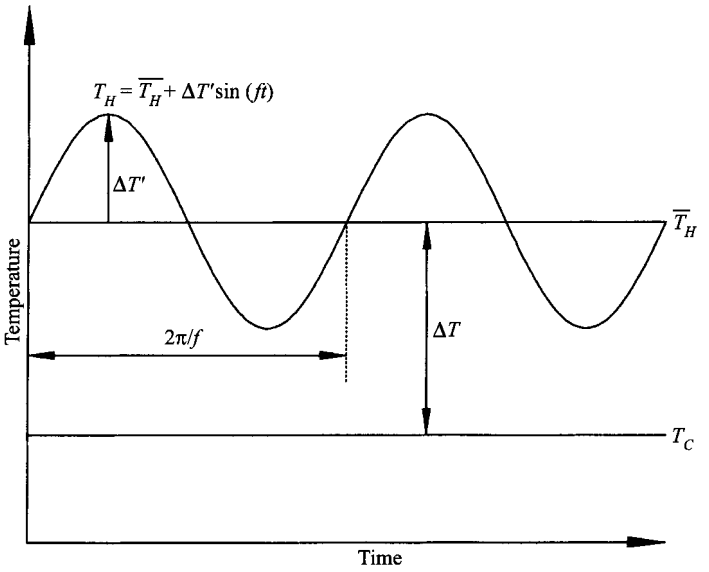

FIGURE 2. Time-dependent temperature boundary condition at the vertical sidewalls.

It should be pointed out that time is made dimensionless, as shown in (6*a*), by referring to the reciprocal of the system Brunt–Väisälä frequency N, i.e.

$$N \equiv [\alpha g(\overline{T_H}-T_C)/H]^{1/2} = (Ra\,Pr)^{1/2}\frac{\kappa}{H^2}. \tag{7}$$

The relevant parameters, in addition to the already-defined Ra and Pr, are

$$\epsilon \equiv \Delta T'/(\overline{T_H}-T_C), \quad \omega \equiv f/N, \tag{8a, b}$$

which are the non-dimensional amplitude and frequency of the wall temperature oscillation, respectively.

		$Pr > 1$	$Pr < 1$
Length	Vertical viscous boundary layer thickness, δ_V	$Ra^{-1/4} Pr^{1/2} H$	$(Ra\,Pr)^{-1/4} H$
	Vertical thermal boundary layer thickness, δ_T	$Ra^{-1/4} H$	$Ra^{-1/4} Pr^{1/4} H$
	Horizontal viscous boundary layer thickness, δ_H	$Ra^{-3/16} A^{-1/4} H$	$(Ra\,Pr)^{-3/16} A^{-1/4} H$
Velocity	Longitudinal velocity in the vertical boundary layer, v_V	$Ra^{1/2} \frac{\kappa}{H}$	$(Ra\,Pr)^{1/2} \frac{\kappa}{H}$
	Horizontal velocity in the horizontal viscous layer, v_H	$Ra^{7/16} A^{1/4} \frac{\kappa}{H}$	$(Ra\,Pr)^{7/16} A^{-1/4} \frac{\kappa}{H}$
Time	Vertical boundary layer formation time, $t_B[\tau_B]$	$Ra^{-1/2} \frac{H^2}{\kappa}[Pr^{1/2}]$	$(Ra\,Pr)^{-1/2} \frac{H^2}{\kappa}[1]$
	Convective time, $t_F[\tau_F]$	$Ra^{-1/4} A^{-1} \frac{H^2}{\kappa}$ $[A^{-1} Ra^{1/4} Pr^{1/2}]$	$Ra^{-1/4} Pr^{-3/4} A^{-1} \frac{H^2}{\kappa}$ $[A^{-1} Ra^{1/4} Pr^{-1/2}]$
	Diffusion time, $t_D[\tau_D]$	$A^{-2} \frac{H^2}{K}$ $[A^{-2} Ra^{1/2} Pr^{1/2}]$	$A^{-2} \frac{H^2}{\kappa}$ $[A^{-2} Ra^{1/2} Pr^{1/2}]$

TABLE 1. The relevant scales for unsteady natural convection in a sidewall-heated cavity. The quantities in square brackets denote dimensionless scales by using the non-dimensionalizations of (6)

3. Numerical computations

The system of equations (1)–(5) was solved numerically by employing a finite-volume procedure based on the SIMPLER algorithm (Patankar 1980). The governing equations were discretized on a staggered grid. Spatial differencing schemes of second-order accuracy were adopted for the equation terms. A central differencing was used for the diffusion terms, and a recently modified version of the QUICK scheme was utilized for calculating the nonlinear convective terms (Hayase, Humphery & Grief 1992). All of the boundary conditions were also treated by using second-order differencing to maintain the same accuracy in the whole computational domain.

The time integration was performed by using an interactive Eulerian implicit method of accuracy $O(\Delta\tau)$. The convergence of the solutions was declared at each time step when the maximum relative change between two consecutive iteration levels falls below 10^{-4} for U, V and θ. A parallel checking was performed to ensure that mass continuity in every computational control volume was satisfied within a relative error 10^{-8}.

For all the calculations discussed in this paper, a grid with (62×52) mesh points in the (X, Y) domain was selected. To resolve thin boundary layers adjacent to the solid walls, grid stretching was implemented such that at least five grid points were located in a boundary layer. A more severe grid clustering was adopted for the horizontal grid than for the vertical one. The present grid resolution was adequate to delineate the boundary-layer structure, although it may not be sufficient to identify the boundary-layer waves (Le Quéré 1990). However, for the present parameter ranges of Ra and Pr, the boundary layer waves are not of major concern (see e.g. Paolucci & Chenoweth

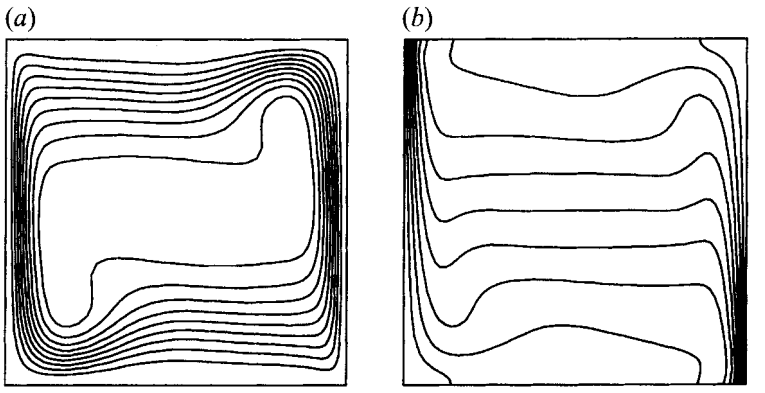

FIGURE 3. (*a*) Streamfunctions and (*b*) isotherms of the basic state ($\epsilon = 0$) for $Ra = 10^6$ and $Pr = 0.7$. The increment of contour level $\Delta\psi$ is $\psi_{max}/10$ and the value of ψ_{max} is listed in table 2. $\Delta\theta = 0.1$.

		Results for the basic state ($\epsilon = 0.0$)			
Pr	Ra	ψ_{max}	Nu	C_i evaluated at $X = 0.5$	Resonance frequency ω_r
0.07	10^5	9.2395×10^{-2}	3.8103	0.8349	0.80
0.07	10^6	4.7024×10^{-2}	7.0342	0.8674	0.70
0.7	10^5	3.6223×10^{-2}	4.5154	0.9560	0.68
0.7	10^6	2.0011×10^{-2}	8.8107	0.9810	0.68
0.7	10^7	1.1347×10^{-2}	16.495	0.9597	0.67
7.0	10^5	1.3188×10^{-2}	4.7190	0.8635	0.55
7.0	10^6	7.4000×10^{-3}	9.2153	0.8006	0.57
7.0	10^7	4.1044×10^{-3}	17.304	0.7738	0.56

TABLE 2. Summary of the present numerical simulations. C_i indicates the strength of interior stratification

1989). Extensive grid sensitivity tests were carried out, and the outcome showed that the reliability and accuracy of the present methodologies were sufficient to capture the principal features, both in the boundary layers and in the core. A very small time step $\Delta\tau = 2\pi/1024\omega$, i.e. 1024 time steps per period, was used.

Verification of the present numerical model was achieved by repeating calculations for the classical model of Patterson & Imberger (1980). For several values of Ra and Pr, the transient behaviour of the flow and heat transfer of the present results was in close agreement with the prior works (e.g. Patterson & Imberger 1980; Patterson & Armfield 1990).

Full numerical computations were done for $Ra = 10^5$, 10^6, and 10^7; $Pr = 0.07$, 0.7, and 7.0 and $0.01 \leqslant \omega \leqslant 10.0$, and for the aspect ratio 1.0. The non-dimensional amplitude ϵ of the wall temperature oscillation was set at $\epsilon = 0.1$; this choice was made so that the oscillating part of the wall temperature would not seriously alter the characteristic regime of the basic flow (Kazmierczak & Chinoda 1992). For each set of (Ra, Pr) pairs, more than 20 computations, using different values of ω, were executed.

Here, it is helpful to have an overview of the physical significance of the parameters selected in this work. The preceding studies provided order-of-magnitude estimates of the scales of the relevant physical variables pertinent to the canonical models of time-dependent convection in a sidewall-heated cavity (e.g. Patterson & Imberger 1980;

Lage & Bejan 1991). These scales are summarized in table 1. Obviously, for all the combinations of (Ra, Pr), the flow regime of present concern is of the boundary-layer type. A major feature of this flow regime is the inseparable coupling between the interior core and the boundary layers on the solid walls (e.g. Jischke & Doty 1975). The time-dependent buoyant motion, in response to the changes in the sidewall thermal conditions, is characterized by three time scales (e.g. Sakurai & Matsuda 1972; Jischke & Doty 1975; Hyun 1994). The shortest, τ_B, is for the formation of the boundary layers on the vertical sidewalls, and in the present non-dimensionalization scheme, $\tau_B \sim O(1)$. The longest time scale, τ_D, represents the diffusion time, and $\tau_D \sim O(Ra^{1/2})$. The intermediate one is the convective time scale, $\tau_F \sim O(Ra^{1/4})$, over which much of the fluid in the cavity passes through the vertical boundary layers. The dominant time-dependent motion, including the process of thermal adjustment in the interior by convective core filling, is substantially accomplished over τ_F.

In view of the parameter ranges selected in the present work, $0.01 \leqslant \omega \leqslant 10.0$, the above-mentioned time scales are comprehensively included in the analysis.

The numerical data are processed to obtain the instantaneous Nusselt number Nu, averaged over a vertical plane at $X = a$:

$$Nu_{X=a} = \frac{L}{H}\int_0^1 \left[U\theta(Ra\,Pr)^{1/2} - \frac{\partial\theta}{\partial X}\right]_{X=a} \mathrm{d}Y. \tag{9}$$

Here, it is advantageous to introduce several operators. In order to assess the impact of the oscillation relative to the corresponding non-oscillating value, a definition is made:

$$\phi^* = \frac{\phi - \phi_{ss}}{\phi_{ss}}, \tag{10}$$

where ϕ represents any time-dependent property, and the subscript ss denotes the corresponding value in the case of non-oscillating wall temperature ($\epsilon = 0$). The amplitude $A(\phi)$ and the mean value $\bar{\phi}$ of an oscillating property over a cycle may be written as

$$A(\phi) = \frac{\mathrm{Max}\{\phi(\tau)\} - \mathrm{Min}\{\phi(\tau)\}}{2} \quad \text{for} \quad \tau_0 \leqslant \tau \leqslant \tau_0 + \frac{2\pi}{\omega}, \tag{11a}$$

$$\bar{\phi} = \left(\int_{\tau_0}^{\tau_0+2\pi/\omega} \phi(\tau)\,\mathrm{d}\tau\right) \Big/ (2\pi/\omega). \tag{11b}$$

In the course of actual computations, a steady-state solution was first procured for a given pair of (Ra, Pr) by setting $\epsilon = 0$. This is referred to as the basic state, which is summarized in table 2. The streamfunction ψ is defined in a usual way, i.e. $U = \partial\psi/\partial Y$, $V = -\partial\psi/\partial X$. Subsequently, this basic state was used as the initial condition for computing the time-varying wall temperature conditions ($\epsilon \neq 0$). This approach, used by Lage & Bejan (1993), saves a considerable amount of numerical effort, in particular for high frequencies. Figure 3 recapitulates the well-established features of the basic-state flow for $Ra = 10^6$ and $Pr = 0.7$ (see e.g. de vahl Davies & Jones 1983). Clearly, the global flow field can be divided into the well-stratified interior core and the boundary layers on the solid walls. The majority of fluid transport is accomplished via the boundary layers, and the interior core is characterized by a stable stratification.

4. Results and discussion

4.1. *Quasi-periodic natural convection responding to the oscillatory thermal boundary condition*

Figure 4 portrays the temporal behaviour of Nu^*, as defined in (10) at three locations, i.e. the cold sidewall (Nu_C^*), the vertical mid-plane $X = 0.5$ (Nu_M^*), and the hot sidewall (Nu_H^*).

Figure 4(*a*) typifies the case of small $\omega(\omega = 0.01)$. It is immediately clear that, only after about one cycle, the values of Nu^* settle down to a form very close to a sinusoidal oscillation. It is also important to notice that the Nu^*-values throughout the entire cavity vary with time almost in unison, i.e. with roughly the same amplitude and in phase. This reflects the fact that the period of the wall temperature oscillation, $\tau_P \equiv 2\pi/\omega$, is much larger than the characteristic time for dominant adjustment of the interior fluid. In other words, since the temporal change in the wall thermal condition is very slow, the flow in the entire cavity at every instant behaves like a time-invariant system. The small phase lags discernible in figure 4(*a*) indicate the time delays for the thermal disturbances originated at the hot wall to reach the position under consideration.

Figure 4(*b*), for a high frequency ($\omega = 10.0$), displays the quasi-steady periodic states. In this case, the shortest time scale τ_B needed for a temperature disturbance to propagate through a distance δ_T, which is the thickness of the thermal boundary layer, by conduction is greater than τ_P. Consequently, over τ_P, the effect of the hot-wall temperature oscillation cannot penetrate across even the vertical boundary layer thickness. The fluctuations of Nu_C and of Nu_M are negligible in magnitude, whereas Nu_H oscillates with an amplitude comparable to the basic-state Nusselt number. The impact of the oscillating temperature wall condition is confined to a narrow region adjacent to the hot wall. This physical picture can be inferred from the well-established Stokes second problem (e.g. Schlichting 1968).

Figure 4(*c*), at an intermediate value of ω, is paradigmatic of a resonant case. The Nusselt numbers everywhere in the cavity show oscillations, although the amplitudes vary spatially. The quasi-steady periodic state is achieved after a few cycles. It is important to notice in figure 4(*c*) that the amplitude of Nu_M is larger than that of Nu_H, i.e. the fluctuation in heat transfer is more vigorous in the interior core than near the hot wall at which the temperature oscillation is applied. Recall that $\epsilon = 0.1$; however, the gain in resulting heat transfer at the mid-plane reaches nearly 35% of the corresponding basic state, i.e. $A(Nu_M^*) = 0.345$.

Figure 5 exhibits the behaviour of the interior velocity, by plotting temporal variations of maximum streamfunction ψ_{max}^*. The response of the flow field is in line with that of heat transfer. The impact of the wall temperature oscillation is moderate for low frequency (see figure 5*a* for $\omega = 0.01$), but is negligibly small for high frequency (see figure 5*b* for $\omega = 10.0$). Very close to the resonance condition, the velocity fluctuations are amplified (see figure 5*c*). Note the difference in the scales of the ordinates in figures 5(*a*), 5(*b*) and 5(*c*).

It is also worth pointing out that the shape of the ψ_{max}^*-curves in figure 5 suggests the presence of the primary mode, which corresponds to ω, plus subsidiary modes. For low ω, the primary mode dominates. However, at high ω, the influence of subsidiary modes is more conspicuous: figure 5(*b*) shows that a quasi-steady mono-periodic state has not been attained even after nearly 40 cycles, and ψ_{max} vacillates with a multitude of frequencies.

Figure 6 (for $Ra = 10^6$, $Pr = 0.7$) illustrates the effect of ω on the global flow and

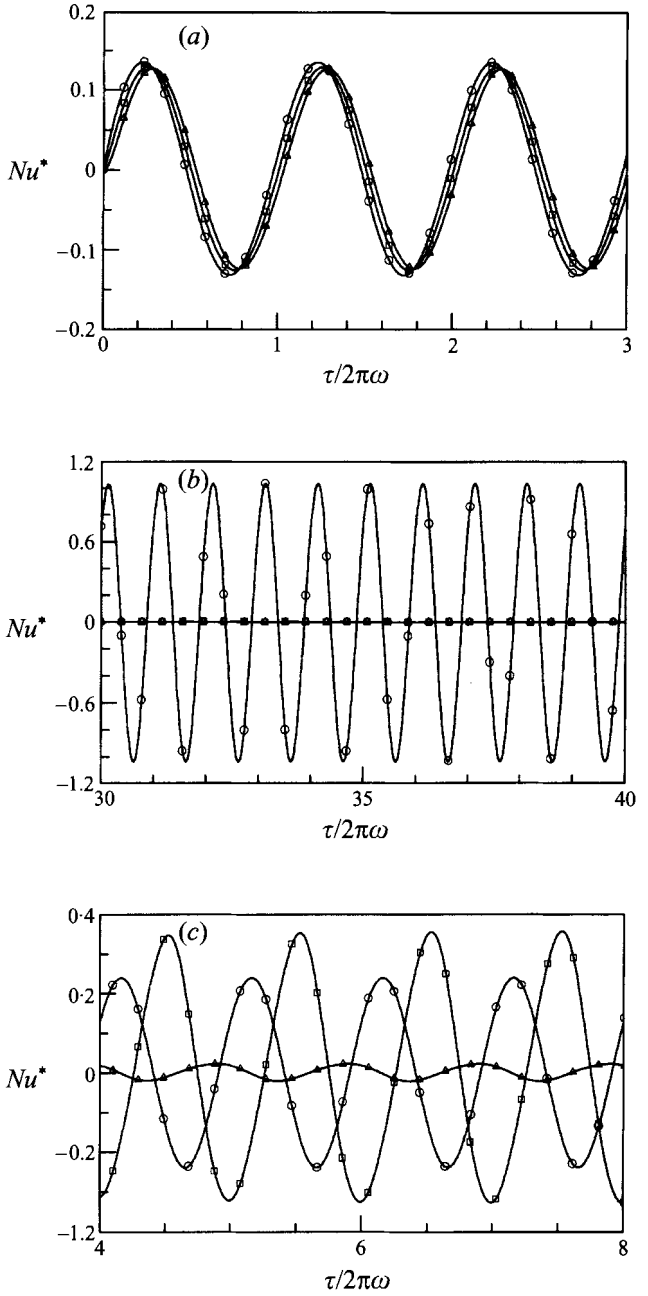

FIGURE 4. Time-dependent behaviour of the overall Nusselt number for $Ra = 10^6$ and $Pr = 0.7$: (*a*) $\omega = 0.01$; (*b*) $\omega = 10.0$; (*c*) $\omega = 0.68$. Symbols ○, □, and △ represent the Nusselt numbers at the hot vertical wall ($X = 1.0$), at the vertical mid-plane ($X = 0.5$), and at the cold vertical wall ($X = 0$), respectively. Note that * denotes a quantity normalized by using (10).

heat transfer characteristics in the quasi-steady periodic state. Figures 6(*a*), 6(*b*) and 6(*c*) plot the amplitude of Nu^* at three locations. A useful approach proposed by Lage & Bejan (1993) was adopted in that resonance in the present natural convection problem is characterized by a maximum fluctuation in the total heat transfer rate through the vertical mid-plane of the cavity. This is also coupled with the occurrence

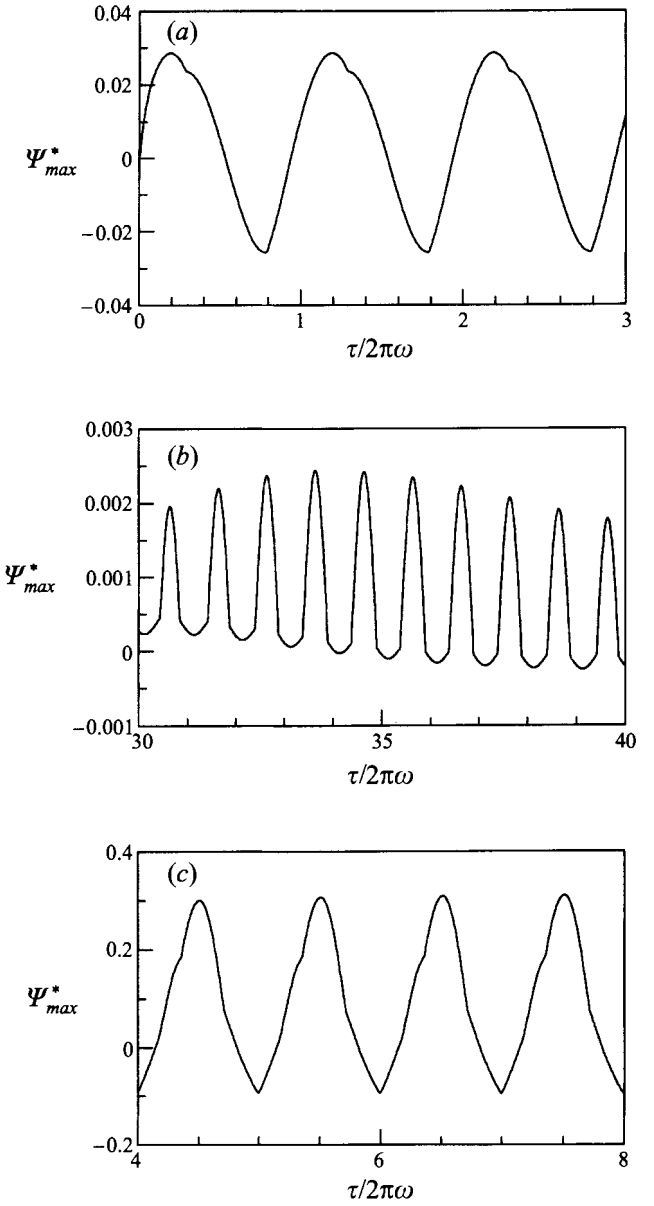

FIGURE 5. Time-dependent behaviour of the normalized maximum streamfunction ψ^*_{max} for $Ra = 10^6$, and $Pr = 0.7$: (*a*) $\omega = 0.01$; (*b*) $\omega = 10.0$; (*c*) $\omega = 0.68$.

of maximum fluctuations in local velocity and temperature of the enclosed fluid. Iwatsu *et al.* (1992) followed a conceptually similar path. Here, the resonance frequency, ω_r, is the frequency at which the amplitude of the Nu_M fluctuation shows a peak value. These are listed in table 2.

The presence of resonance is corroborated in figure 6(*b*), with the resonance frequency $\omega_r \approx 0.68$. At low frequencies, $A(Nu^*_M)$ remains nearly constant. In a narrow band surrounding ω_r, $A(Nu^*_M)$ is substantially amplified, with a peak value at ω_r. As ω increases beyond ω_r, $A(Nu^*_M)$ decreases rapidly to approach zero.

The dependence of the fluctuations of Nu_H and Nu_C on ω is displayed in figures 6(*a*)

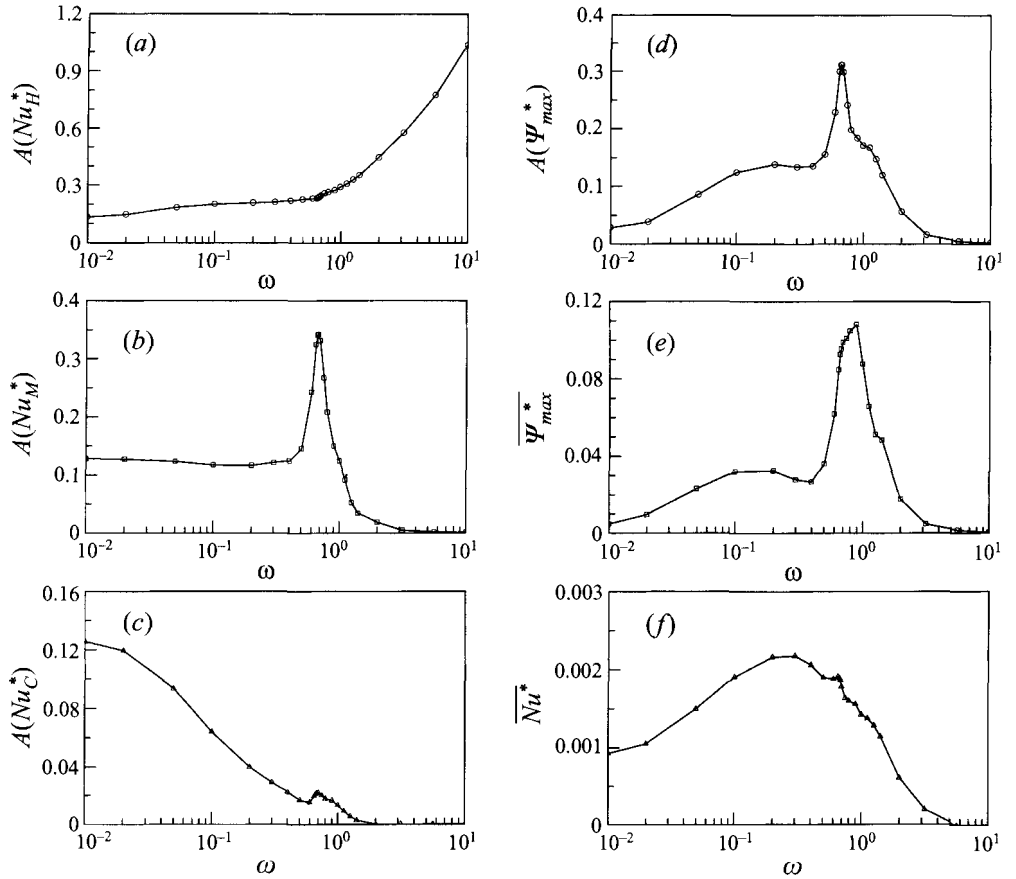

FIGURE 6. Variations of the fluctuations of flow variables with ω. (*a*) $A(Nu_H^*)$ at $X = 1.0$; (*b*) $A(Nu_M^*)$ at $X = 0.5$; (*c*) $A(Nu_C^*)$ at $X = 0$; (*d*) $A(\psi_{max}^*)$; (*e*) $\overline{\psi_{max}^*}$; and (*f*) $\overline{Nu^*}$. $Ra = 10^6$, $Pr = 0.7$.

and 6(*c*), respectively. For $\omega < \omega_r$, the fluctuation of Nu_H generally increases with frequency while that of Nu_C decreases. Note the difference in scales of the ordinates of figure 6(*a*) and figure 6(*c*). As ω increases beyond ω_r, $A(Nu_H^*)$ increases steeply, whereas $A(Nu_C^*)$ becomes very small. A less distinctive peak is visible in the plot of $A(Nu_C^*)$ at $\omega \approx \omega_r$. Figure 6(*d*) exhibits the dependence of velocity fluctuations on ω. Resonance, as exemplified by a peak value of $A(\psi_{max}^*)$, is in evidence. Clearly, the value of the time-dependent ψ_{max} (for $\epsilon = 0.1$) is enhanced to about 31% above the basic-state ψ_{max} (for $\epsilon = 0$).

The effect of ω on the cycle-averaged values of $\overline{\psi_{max}^*}$ and $\overline{Nu^*}$ is depicted in figures 6(*e*) and 6(*f*). In general, the influence of the wall temperature oscillation on $\overline{\psi_{max}^*}$ is small in comparison to that on $A(\psi_{max}^*)$. Note the difference between the scales of the ordinates of figures 6(*d*), 6(*e*) and 6(*f*). It is difficult to draw any definitive conclusion at present, but it is conjectured that such a relatively small impact on the averaged quantities may stem from the fact that $\epsilon = 0.1$ in the present computations. This amplitude of the wall temperature oscillation is not sufficient to seriously disturb or alter the structures of the time-averaged flow and temperature fields.

The effects of *Ra* and *Pr* are shown in figure 7, by executing calculations for all the sets of (*Ra*, *Pr*) listed in table 2. Although the results display quantitative differences, as anticipated, the overall qualitative features remain substantially unchanged. For all the cases computed, the existence of distinctive resonance is reconfirmed, and this trend

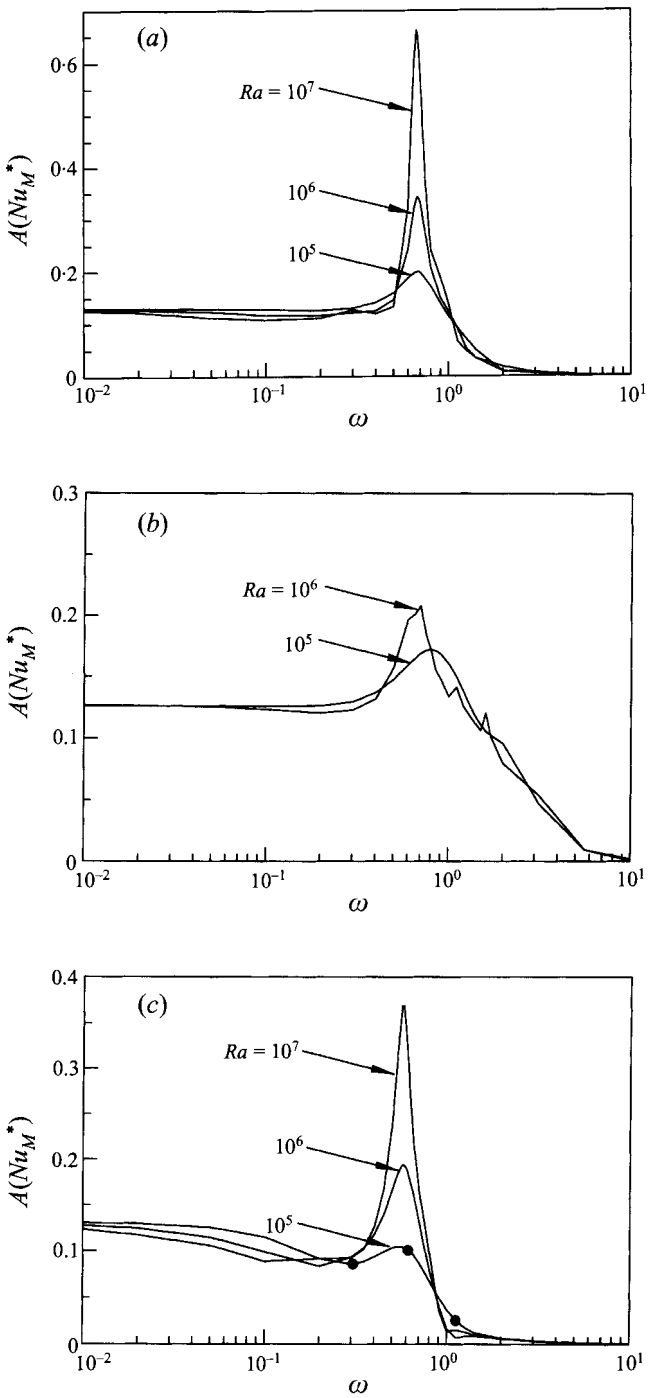

FIGURE 7. Effects of Ra and Pr on the $A(Nu_M^*)$ variation with ω. (*a*) $Pr = 0.7$, (*b*) $Pr = 0.07$, (*c*) $Pr = 0.7$. The solid circles in (*c*) are results from Kazmierczak & Chinoda (1992).

becomes more pronounced as Ra increases. When Ra is relatively small (see the curves for $Ra = 10^5$), resonance is less clear-cut. Also, $A(Nu_M^*)$ is nearly independent of Ra at low frequencies, and becomes vanishingly small at high frequencies. The influence of Ra is mainly felt only in a narrow frequency band surrounding ω_r, which is termed the

resonance band. Within this frequency band, the fluctuation of Nu_M^* is notably amplified as Ra increases.

The effect of Pr is also shown in figure 7. The general qualitative patterns of the $A(Nu_M^*)$ vs. ω curves are similar. For a very small value of Pr, as shown in figure 7(*b*) for $Pr = 0.07$ and $Ra = 10^6$, the secondary and third peaks are visible. These subsidiary peaks are thought to be the harmonics of the fundamental frequency ω_r. Another important observation is that, for the same Ra, $A(Nu_M^*)$ for $Pr = 0.7$ is much greater than that for $Pr = 0.07$ or for $Pr = 7.0$. A plausible explanation may be given based on physical grounds. The ultimate source of the resonance in the natural convection is the thermal disturbances excited by the hot-wall temperature oscillation. These disturbances are then transported via convective currents. A departure from $Pr = 1$ implies unequal damping by viscosity and thermal diffusion effects. For $Pr > O(1)$, viscous diffusion is the major damping mechanism for the propagation of the disturbances, whereas for $Pr < O(1)$ thermal diffusion weakens the thermal disturbances. Consequently, for a fluid of $Pr \sim O(1)$, resonance is expected to generate most dramatic consequences. This can also be ascertained from the results of Lage & Bejan (1993), which showed that for a fixed Ra, the fluctuation of Nu was most amplified for $Pr \sim O(1)$.

It is now of interest, in the light of the present comprehensive numerical results, to recast the earlier study of Kazmierczak & Chinoda (1992) in terms of the same problem set-up. As remarked previously, they used larger values of ϵ, i.e. $\epsilon = 0.2$, 0.4, and 0.8. However, their numerical solutions reported a monotonic dependency of the fluctuations in flow and heat transfer on ω, and no explicit resonance was seen. It can be shown that their failure to capture resonance was attributable to the extreme limitations of the parameter values of their computations and to the poor resolution of frequency bands. The only pair of (Ra, Pr) chosen in their study was $Ra = 1.5 \times 10^5$, $Pr = 7.0$. Unfortunately, for this choice the resonant convection is generally feeble (see the present results for $Ra = 10^5$, $Pr = 7.0$ in figure 7*c*). On top of this, their computations encompassed only three different values of frequency. In terms of the present non-dimensionalization, their run nos. 1, 4 and 5 correspond to $\omega = 0.6132$, 1.1226 and 0.3066, respectively, in the present study. These results are indicated in figure 7(*c*) as solid circles which shows that they are too coarse to capture any sign of a peak around $\omega_r \approx 0.56$. In fact, a closer perusal of figures 6 and 13 of Kazmierczak & Chinoda (1992) suggests that the fluctuation of Nu_M at $\omega = 0.6132$ is slightly more intensified than the other two cases. This observation is consistent with the present results demonstrated in figure 7(*c*).

4.2. *Identification of the resonance frequency*

Lage & Bejan (1993), by using the concept of the rotation of a fluid wheel, stated that resonance is expected if the period of oscillation of the external boundary condition coincides with the time taken for the effect of cyclic heating to rotate through the full cavity. The period t_W of one rotation of a fluid wheel was scaled as

$$t_W \sim 4H/V_0, \tag{12}$$

in which the fluid rotates like a wheel of diameter H with velocity V_0. These baseline physical considerations are similar to the case of a driven pendulum; t_W is associated with the natural frequency of the pendulum.

Subsequently, Lage & Bejan used the longitudinal velocity in the vertical boundary layer to estimate V_0 in (12). This scaling emphasizes the significance of the boundary layer structure of the basic state, in the belief that the bulk of the fluid transport in the

basic state is achieved through the boundary layers. Therefore, in this model, the impact of the oscillating thermal boundary condition travels is through circulations of the basic state through the boundary layers. Cementing these arguments, the non-dimensional resonance frequency may be expressed as

$$\omega_r = \begin{cases} \frac{1}{2}\pi & \text{for} \quad Pr < 1, \\ \frac{1}{2}\pi Pr^{-1/2} & \text{for} \quad Pr \geqslant 1. \end{cases} \tag{13}$$

A small modification to (13) may now be obtained. Taking into account both the transverse velocity in the horizontal boundary layer and the longitudinal velocity in the vertical boundary layer, (13) can be rewritten in a slightly amended form:

$$\omega_r = \begin{cases} \dfrac{\pi}{1+(Ra\,Pr)^{1/6}} & \text{for} \quad Pr < 1, \\ \dfrac{\pi}{Pr^{1/2}(1+Ra^{1/6})} & \text{for} \quad Pr \geqslant 1. \end{cases} \tag{14}$$

The heuristic scale analysis approach of Lage & Bejan (1993) will now be slightly modified and expanded to incorporate the numerical results of the present computations. It was found, as shown in figure 7, that both the resonance frequency ω_r and the width of the resonance band are little affected by Ra and Pr. Only the case of $Pr = 0.07$ is there a slight variance with Ra. The effects of Pr on ω_r are also weak. Recalling that time was made dimensionless by using $1/N$, these findings suggest that resonance is closely linked to internal gravity wave oscillations.

As stated earlier, it is essential to identify the eigenmodes of oscillations of the system. Several oscillatory modes of natural convection in a sidewall-heated cavity have been discussed (Patterson & Imberger 1980; Ivey 1984; Le Quéré & Alziary de Roquetfort 1986; Paolucci & Chenoweth 1989; Le Quéré 1990; Xia *et al.* 1995). Paolucci & Chenoweth (1989) calculated the frequencies of the internal wave oscillation and boundary-layer wave oscillations. The frequency of internal wave oscillation suggested by them is, in dimensional form,

$$f^I = C_i \frac{N}{[A+(n/q)^2/A]^{1/2}}, \tag{15}$$

where C_i is a parameter indicating the strength of stratification, and q and n are the wavenumbers in the horizontal and vertical directions, respectively. For the fundamental mode, $A = 1.0$, $n/q = 1$ and in the present dimensionless form, they gave

$$\omega^I = \frac{C_i}{\sqrt{2}}. \tag{16}$$

Paolucci & Chenoweth (1989) found that C_i was approximately constant and slightly less than unity for $Pr = 0.71$. In the present study, following Paolucci (1990), the stratification factor, C_i, of the basic state was calculated by using a linear fitting to the vertical temperature distribution at the horizontal mid-width plane of the cavity ($X = 0.5$). This is listed in table 2. The estimated values of C_i for $Pr = 0.7$ are shown to be in good agreement with those obtained by Paolucci & Chenoweth (1989) for $Pr = 0.71$. The order-of-magnitude strength of the overall core stratification remains largely unchanged as Ra and Pr vary. Based on this argument, (16) indicates that the frequency of the internal gravity mode, if scaled by using the Brunt–Väisälä frequency,

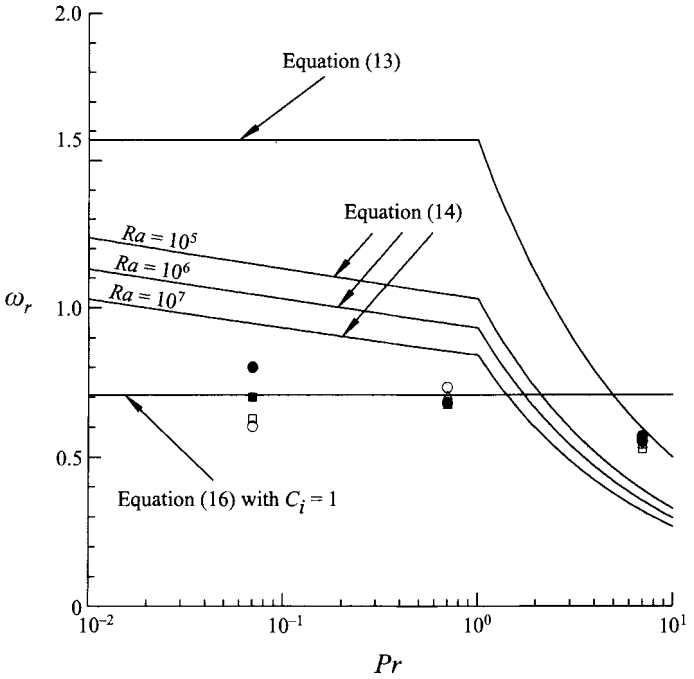

FIGURE 8. Values of the resonance frequency ω_r. The curves are based on the scaling arguments, (13), (14) and (16). ●, ■, ▲ denote the present numerical results for $Ra = 10^5$, 10^6, 10^7, respectively, ○, □, △ represent the values based on (16), when C_i is evaluated by using the vertical temperature distribution of the present numerical results for $\epsilon = 0$ at the mid-width of the cavity.

is nearly constant. This corroborates the foregoing statement that, at resonance, the internal wave oscillations are excited.

The numerically determined values for the resonance frequency ω_r are compiled in figure 8 for all the computational runs of the present study. Also shown in figure 8 are the predictions by (13) and (14). Quantitative discrepancies are seen between the present numerical results and the prediction based on the scaling of Lage & Bejan (1993). It appears that, in line with the statement of Lage & Bejan, the prediction by scale analysis tends to underpredict ω_r for $Pr > O(1)$ and overpredict it for $Pr < O(1)$. It is immediately clear in figure 8 that the present numerical data for ω_r cluster around the frequency ω^I of (16) with $C_i = 1$. Figure 8 also shows the frequency of internal wave oscillations, based on the value C_i in table 2. These illustrate close agreement with the numerical data for ω_r for $Pr \geqslant O(1)$.

Note that, for all the sets of (Ra, Pr) in the present study with $\epsilon = 0$, no oscillatory motions are seen in the steady state. This is consistent with the results of Paolucci & Chenoweth ($\epsilon = 0$); in the range of Ra examined in that paper, the amplitudes of internal wave oscillations eventually decay. However, in the present problem with the periodic thermal boundary condition at the sidewall, a continuous energy source with a frequency close to that of the internal waves is provided, and the internal wave oscillations are maintained due to resonance.

4.3. *Flow response at resonance*

The detailed time-dependent flow and temperature structures at resonance will now be described. In order to gain physical insight into the mechanism of resonance, it is

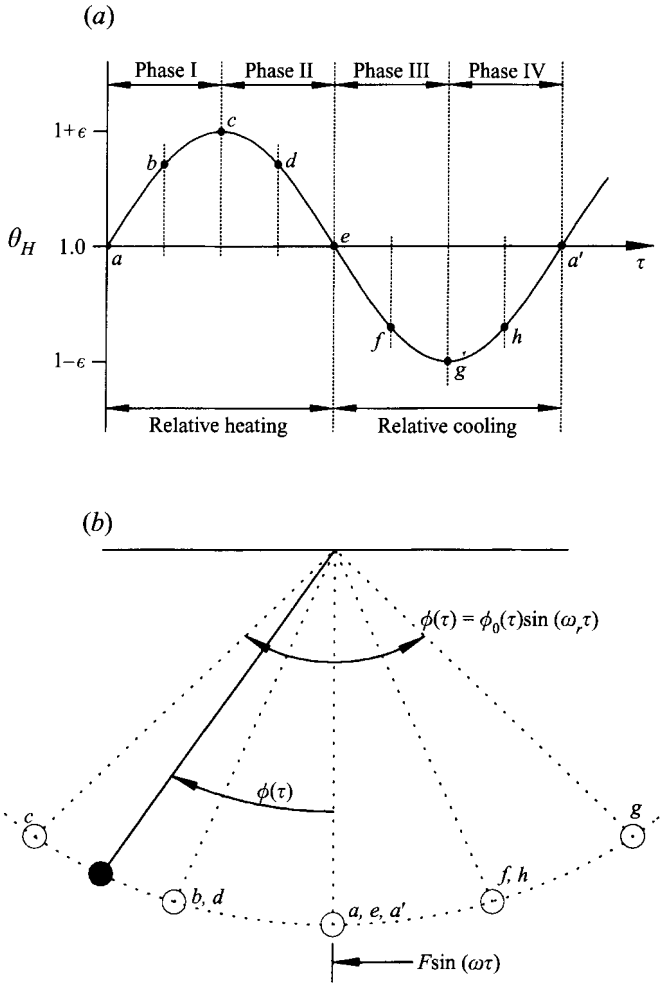

FIGURE 9. (*a*) Characterization of heating and cooling modes relative to the basic state at the hot wall. (*b*) An analogous model of a driven pendulum.

necessary to scrutinize the details of the oscillating components of the flow. This carries added significance in the light of the fact that the oscillatory characteristics are masked by the dominant basic-state features. A thorough and complete analysis will be made of $\psi'(\equiv \psi - \psi_{ss})$ and $\theta'(\equiv \theta - \theta_{ss})$, where the subscript *ss* refers to the basic state ($\epsilon = 0$).

The history of the relative influence of the hot-wall thermal boundary condition is portrayed in figure 9. A cycle is divided into four phases. The first (last) half of a cycle, $\tau_a \leqslant \tau < \tau_e (\tau_e \leqslant \tau < \tau_{a'})$ can be interpreted as a heating (cooling) mode relative to the basic state, since $\theta_H \geqslant \bar{\theta}_H (\theta_H \leqslant \bar{\theta}_H)$. Also, phases I and IV (phases II and III) are characterized by a positive (negative) rate of change of θ_H. An analogy between the present problem and the driven pendulum can be drawn as shown in figure 9(*b*).

Figure 10 displays time-dependent profiles of θ' along the mid-depth plane ($Y = 0.5$) under the resonant condition ($\omega = \omega_r$) for $Ra = 10^6$, $Pr = 0.7$. The global; features of the temperature field, including the structures of thermal boundary layers and core stratification, display little change with time. However, figure 10 reveals the periodic tilting of the interior isotherms. Owing to this oscillatory tilting of the isotherms, the

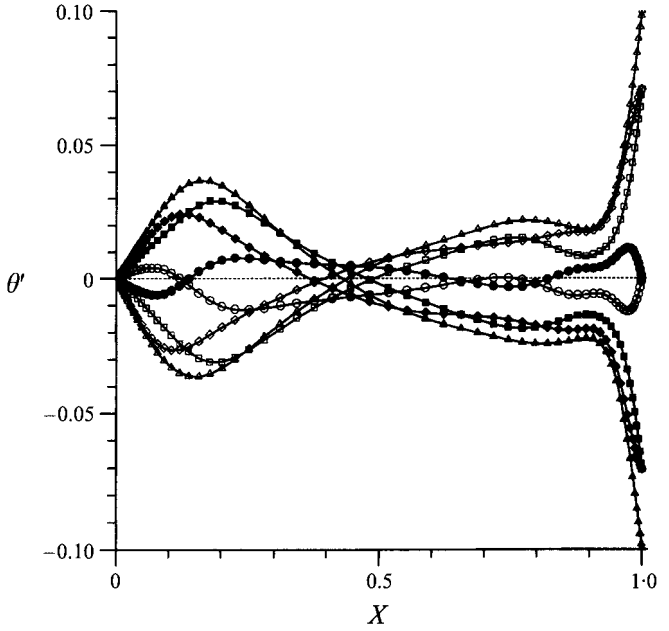

FIGURE 10. Time-dependent profiles of the oscillating temperature component, θ', in the horizontal mid-plane ($Y = 0.5$). $Ra = 10^6$, $Pr = 0.7$ and $\omega = 0.68$. The time instants are: ○, $\tau = \tau_a$; □, $\tau = \tau_b$; △, $\tau = \tau_c$; ◇, $\tau = \tau_d$; ●, $\tau = \tau_e$; ■, $\tau = \tau_f$; ▲, $\tau = \tau_g$; ◆, $\tau = \tau'_a$.

fluid in the interior core experiences a situation as if the gravity vector changes its direction in an oscillatory manner with time. It is stressed that this periodic tilting of the interior isotherms is most pronounced when $\omega \approx \omega_r$. This supports the earlier assertion that the flow resonates with the internal wave oscillations.

Figure 11 (for $Ra = 10^6$, $Pr = 0.7$) exhibits sequential plots of ψ' and θ' for the resonance case. At time $\tau = \tau_a$, the full domain of fluid is occupied by a clockwise (CW) circulating cell, which was developed by the relative cooling in the previous cycle. As θ'_H increases in phase I (see frames *a*, *b*, *c*), a new counterclockwise (CCW) circulation forms near the hot vertical sidewall and this grows to push the CW circulation to the cold-wall side. At $\tau = \tau_c$, the CCW cell occupying the half-cavity is characterized by two centres of circulation (see frame *c*): one is located in the upper right corner and the other is in the central region of the cavity. In phase II (see frames *c*, *d*, *e*), the CCW cell fills most of the cavity, and the two centres of circulation merge into one which moves to the cold-wall side. Around $\tau \approx \tau_e$, the strength of this CCW circulation is maximized. During the relative cooling period ($\tau_e \leqslant \tau \leqslant \tau_{a'}$) a reverse process takes place. In the above-described fashion, in a cycle, the CW and CCW circulating cells are developed and subsequently disappear.

A close inspection of the evolution of θ' gives insight into the resonance. In figure 11(*a*), the appearance of cool spots, which are characterized by negative values of θ', is visible in the upper right corner region. These represent the horizontal intrusion of cold disturbances which were generated under the relative cooling mode of the previous cycle and were transported by buoyant currents in the hot-wall boundary layer. As can be readily observed in figures 11(*b*) and 11(*c*), these cold disturbances do not travel through the upper boundary layer with the convective currents of the basic state; rather, they move across the interior region of the cavity. By the time when the hot disturbances, which are generated subsequently at the hot wall, begin to occupy the

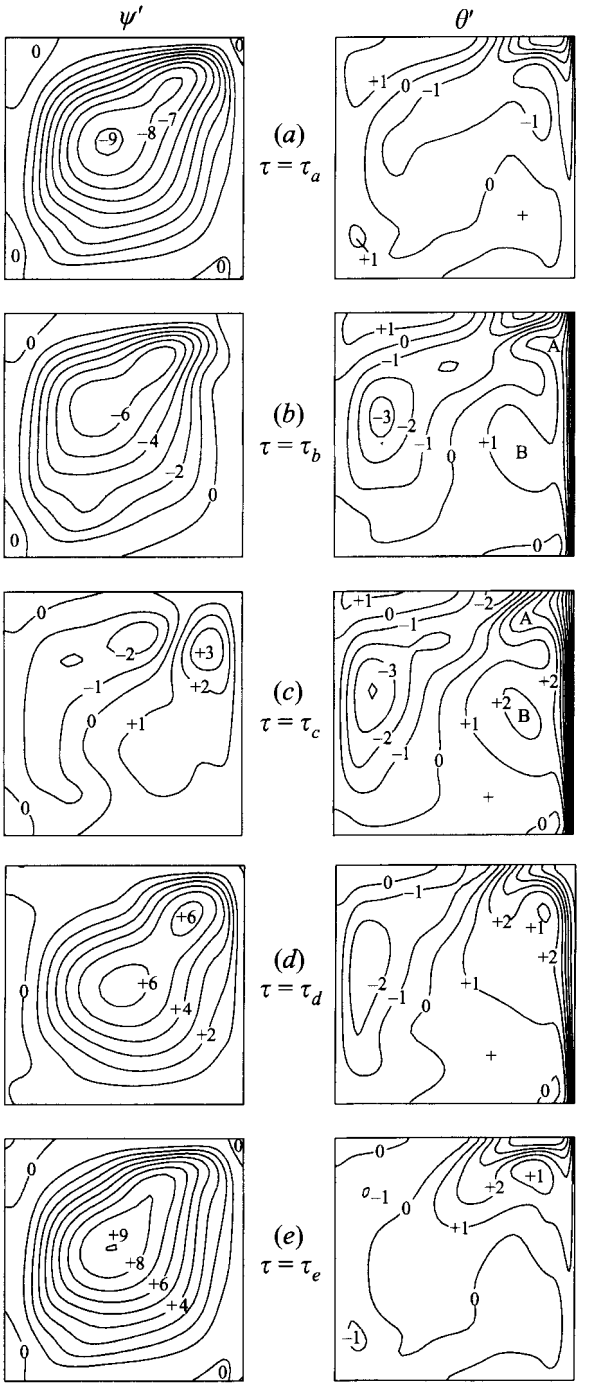

FIGURE 11. Sequential plots showing the oscillating parts of streamfunctions (left column) and of isotherms (right column). $Ra = 10^6$, $Pr = 0.7$, and $\omega = 0.68$ ($\approx \omega_r$). The time instants are as shown in figure 9. The contour increments are $\Delta\psi' = 7.5 \times 10^{-4}$ and $\Delta\theta' = 0.01$. The number, n, in the figures indicates the contour value $n\Delta\psi'$ or $n\Delta\theta'$.

central region of the cavity, the cold disturbances have been divided into two parts. The cold disturbances in the upper zone are isolated and they die out as the succeeding hot fluid replaces them; however, those in the lower zone turn at the cold sidewall and move toward the hot sidewall through the lower region of the cavity. This movement of the cold spot through the lower region, which was generated by the relative cooling of the previous cycle, provides an essential clue to resonant convection.

Following up the above discussion, the effects of relative heating are traced. In figure 11(*a*), around $\tau = \tau_a$, hot disturbances due to the increase in θ_H grow in the hot-wall boundary layer. Notice, in this frame, that another zone of positive θ' (hot spots) is evident in the lower right quarter of the cavity. The appearance of this region is attributable to the above-described returning of the relative heating effects of the previous cycle. Figure 11(*b*) exhibits the presence of two modes of propagation of the hot disturbances: one is in the upper right corner (denoted by region A in figure 11), and the other starts directly from the mid-height of the hot-wall boundary layer (denoted by region B in figure 11). The former represents the intrusion of the fluid parcels which were heated in the present cycle and are transported by the basic-state upwelling buoyant currents in the hot-wall boundary layer. The latter results from the interaction of heating effects of the present cycle with the return of heating effects of the previous cycle. Around $\tau = \tau_c$, these two hot spots propagate into the interior region and they merge into a single zone. This merging intensifies the hot disturbances in the interior core; this pushes to the cold-wall side the cold disturbances which occupy the central portion of the cavity. Afterwards, these hot disturbances travel directly across the bulk of the interior. In a similar manner, cold disturbances are newly created under the relative cooling mode, and these strongly interact with the returning of the cooling effects of the previous cycle. These processes are repeated in every cycle.

This description of the behaviour of oscillating components is analogous to the resonance of a driven pendulum shown in figure 9(*b*). If an external excitation is applied to the pendulum which is initially motionless, the pendulum starts oscillating with its natural frequency, ω_r. If there is no damping, the pendulum continues to oscillate permanently. Suppose that an external forcing is continuously applied to the pendulum at every time instant when the pendulum passes its original position ($\tau = \tau_a$), i.e. the frequency ω of the external forcing is $\omega = \omega_r$. The pendulum gains additional angular momentum, which produces resonance so that the oscillation is amplified. For an ideal system with no damping, the amplitude grows unbounded. In the present fluid system, viscous and diffusive dampings restrict the amplification to an appropriate level. Fluctuations of flow and associated convective heat transfer are intensified most when the effects of the oscillating temperature boundary condition by the previous cycle and by the current cycle are synchronized. If this temporal matching is achieved, maximal effects of the time-varying hot-wall conditions are imparted to the fluid, and this constitutes the grounds for resonance.

The evolution of ψ' and θ' at off-resonance frequencies is displayed in figure 12 (at $\omega = 0.5$) and figure 13 (at $\omega = 1.0$).

When $\omega < \omega_r$, the period of the hot-wall temperature oscillation is larger than the time required for the thermal effects to span the full fluid domain. This is corroborated in figure 12(*a*); at time $\tau = \tau_a$, the presence of CCW circulation is felt in much of the lower half of the cavity. This is in contrast to the picture at $\tau = \tau_a$ of the resonance case (see figure 11*a*), in which CW circulation fills the majority of the cavity interior. CW circulation, in the case of $\omega < \omega_r$, cannot fill the full cavity domain due to the remaining effects of the relative heating of the previous cycle (the relative heating of the new cycle has not yet had an effect). As is readily seen in figures 12(*b*) and 12(*c*), the interaction

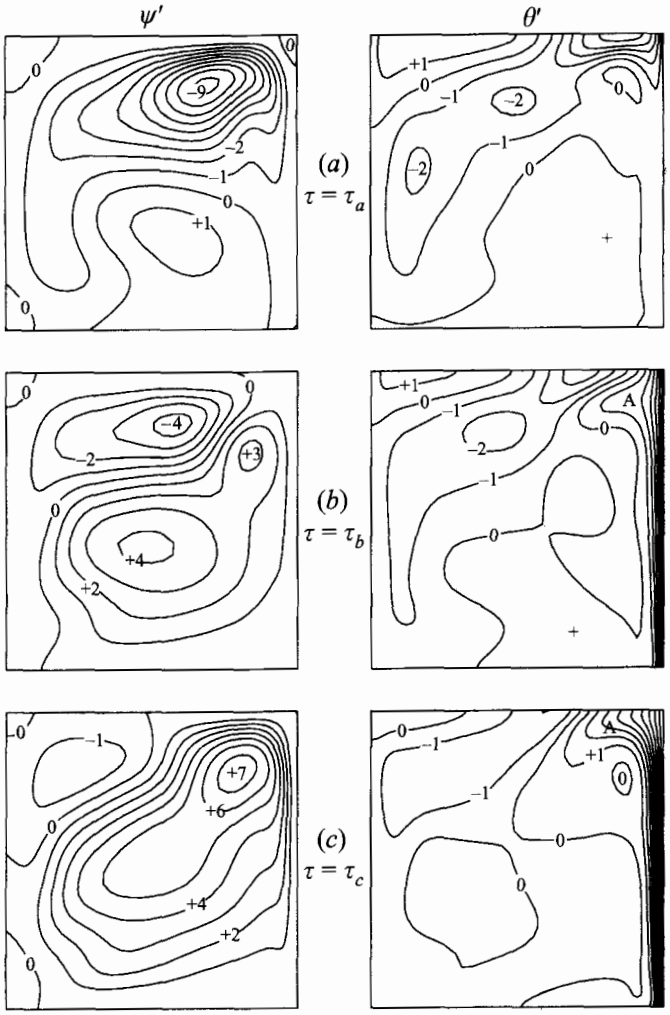

FIGURE 12. Same as in figure 11, but for $\omega = 0.5$ ($< \omega_r$). $\Delta\psi' = 5 \times 10^{-4}$.

between two hot spots of different temporal origins is much weaker than for the resonance case.

Figure 13 (at $\omega = 1.0$) illustrates the results for $\omega > \omega_r$. The period of the change of the wall boundary condition is shorter than the time taken for the thermal effects to span the entire cavity. The ψ'-frame of figure 13(a) shows that a pair of counter-rotating circulation cells is arranged more or less in the horizontal direction. The CW (CCW) circulation in the left (right) half of the cavity represents the residual impacts of the relative cooling (heating) of the previous cycle. The θ'-frames portray similar patterns. At $\tau = \tau_a$, a good part of the left half of the cavity is occupied by hot disturbances (positive θ'), whereas the right half contains mostly cold disturbances (negative θ'). At this instant, the temperature condition at the hot wall has been switched to a relative heating mode; however, the effect of relative heating of the previous cycle has not yet completed its passage across the cavity. Accordingly, the resonant interaction between the relative heating effects of the current and the previous cycles is not in evidence. Rather, as seen in figure 13(c), the horizontally arranged structure of alternating regions of positive and negative θ' inhibits the propagation of

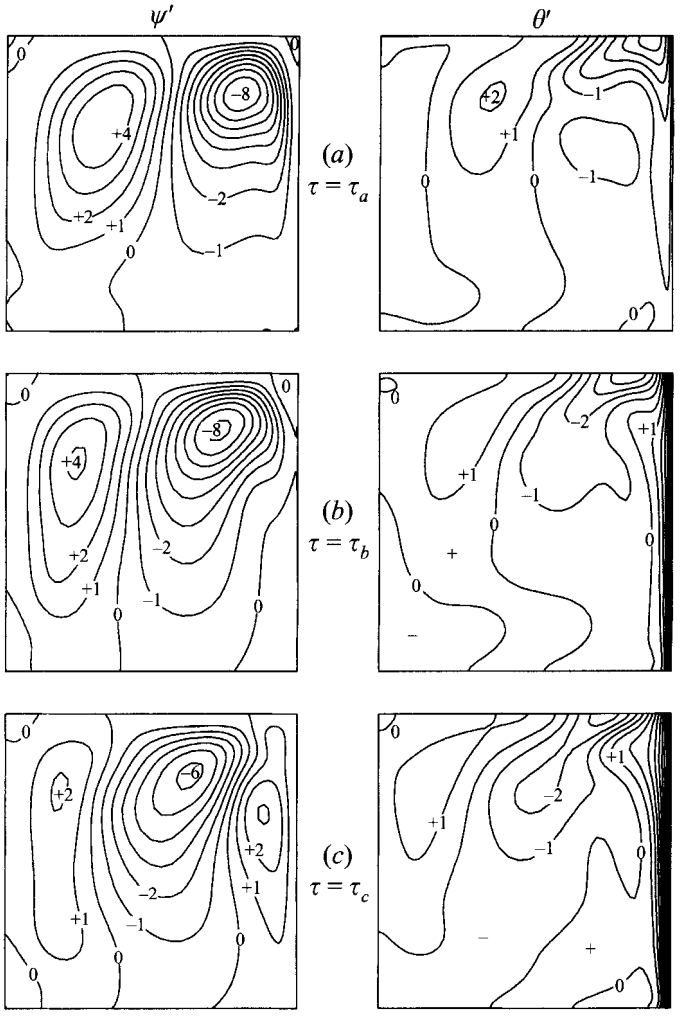

FIGURE 13. Same as in figure 11, but for $\omega = 1.0\ (> \omega_r)$. $\Delta\psi' = 5 \times 10^{-4}$.

the effect of the hot-wall temperature oscillation. Owing to the blocking role of this structure, the impact of the oscillating hot-wall temperature condition of the past cycles cannot reach the hot-wall side. The rapid decline in the fluctuation of Nu_M with ω when $\omega > \omega_r$ (see figures 6 and 7) can be explained by this physical picture.

5. Concluding remarks

Wide-ranging numerical computations have been conducted to study natural convection in a sidewall-heated square cavity with a time-varying temperature boundary condition at the hot sidewall, $\theta_H = 1 + \epsilon \sin(\omega\tau)$. The numerical calculations clearly showed resonance at a selected frequency (ω_r) by monitoring the maximization of fluctuations in the heat transfer rate in the interior region. For $\omega < \omega_r$, the fluid response to the hot-wall temperature oscillation is qualitatively similar to the case of an impulsive step change in temperature given to the boundary wall. For $\omega > \omega_r$, the

influence of the boundary condition is confined to a narrow region adjacent to the hot sidewall.

The resonance phenomenon is more distinct and the amplification of Nu_M is more pronounced as Ra increases for $Pr \sim O(1)$. However, the resonance frequency ω_r, non-dimensionalized by using the system Brunt–Väisälä frequency, is nearly independent of Ra and Pr. In the resonant case, the impact of the hot-wall temperature oscillation is conspicuous in the interior core and the temperature field in the interior core displays a periodic tilting of isotherms. This suggests that the flow investigated here resonates with the internal wave oscillations. Estimations of ω_r based on the internal wave modes are in qualitative agreement with the present numerical results.

The underlying mechanism of resonance is investigated by examining the details of oscillating components of flow and temperature fields. Analogous to the driven pendulum problem, resonance is due to strong interactions between the effects of oscillatory thermal boundary conditions generated by the previous and by the current cycles. The influence of the sinusoidally varying thermal wall condition synchronizes with the returning impact of the wall condition produced in the previous cycle. For a resonant case, CCW and CW circulations in the oscillatory flow field grow and then disappear over a cycle. The thermal disturbances from the hot sidewall move through much of the interior core and return to the original position over a period.

The major motivation of the present study was to search for resonance of natural convection in the sidewall-heated cavity. Relatively small Rayleigh numbers were covered so that the time-invariant steady state exists when $\epsilon = 0$. As reported by Paolucci & Chenoweth (1989), for a higher value of Ra, internal wave oscillations are present even in the steady state. In this situation, it is expected that resonance results in a more dramatic amplification of oscillations. If the value of Ra is much higher, boundary-layer waves may also be activated (Paolucci & Chenoweth 1989; Le Quéré 1990). These are not of major interest in the present study.

Appreciation is extended to the referees whose constructive comments and suggestions led to improvements in the revised version. This work was supported in part by research grants from the Ministry of Science and Technology, Korea.

REFERENCES

BARK, F. H., ALAVYOON, F. & DAHLKILD, A. A. 1992 On steady free convection in vertical slots due to prescribed fluxes of heat or mass at the vertical walls. *J. Fluid Mech.* **235**, 665–689.

CHENOWETH, D. R. & PAOLUCCI, S. 1986 Natural convection in an enclosed vertical air layer with large horizontal temperature differences. *J. Fluid Mech.* **169**, 173–210.

DAVIS, G. DE VAHL & JONES, I. P. 1983 Natural convection in a square cavity – a comparison exercise. *Intl J. Num. Methods Fluids* **3**, 227–248.

HAYASE, T., HUMPHERY, J. A. C. & GRIEF, R. 1992 A consistently formulated QUICK scheme for fast and stable convergence using finite-volume iterative calculation procedures. *J. Comput. Phys.* **98**, 108–118.

HYUN, J. M. 1994 Unsteady buoyant convection in an enclosure. *Adv. Heat Transfer* **34**, 277–320.

IVEY, G. N. 1984 Experiments on transient natural convection in a cavity. *J. Fluid Mech.* **144**, 389–401.

IWATSU, R., HYUN, J. M. & KUWAHARA, K. 1992 Convection in a differentially-heated square cavity with a torsionally-oscillating lid. *Intl J. Heat Mass Transfer* **35**, 1069–1076.

JISCHKE, M. C. & DOTY, R. T. 1975 Linearized buoyant motion in a closed container. *J. Fluid Mech.* **71**, 729–754.

KAZMIERCZAK, M. & CHINODA, Z. 1992 Buoyancy-driven flow in an enclosure with time-periodic conditions. *Intl J. Heat Mass Transfer* **35**, 1507–1518.

LAGE, J. L. & BEJAN, A. 1991 The *Ra–Pr* domain of laminar natural convection in an enclosure heated from the side. *Numer. Heat Transfer* A **19**, 21–41.

LAGE, J. L. & BEJAN, A. 1993 The resonance of natural convection in an enclosure heated periodically from the side. *Intl J. Heat Mass Transfer* **36**, 2027–2038.

LE QUÉRÉ, P. 1990 Transition to unsteady natural convection in a tall water-filled cavity. *Phys. Fluids* A **2**, 503–514.

LE QUÉRÉ, P. & ALZIARY DE ROQUETFORT, T. 1986 Transition to unsteady natural convection of air in differentially heated vertical cavities. *Proc. ASME Winter Annual Meeting, Anaheim, California.* ASME HTD, Vol. 60, pp. 29–36.

OSTRACH, S. 1982 Natural convection heat transfer in cavities and cells. *Proc. 7th Intl Heat Transfer Conf., Munich*, Vol. 6, pp. 365–379.

PAOLUCCI, S. 1990 Direct numerical simulation of two-dimensional turbulent natural convection in an enclosed cavity. *J. Fluid Mech.* **215**, 229–262.

PAOLUCCI, S. & CHENOWETH, D. R. 1989 Transition to chaos in a differentially heated vertical cavity. *J. Fluid Mech.* **201**, 379–410.

PATANKAR, S. V. 1980 *Numerical Heat Transfer and Fluid Flow.* McGraw-Hill.

PATTERSON, J. & ARMFIELD, S. W. 1990 Transient features of natural convection in a cavity. *J. Fluid Mech.* **219**, 469–497.

PATTERSON, J. & IMBERGER, J. 1980 Unsteady natural convection in a rectangular cavity. *J. Fluid Mech.* **100**, 65–86.

SAKURAI, T. & MATSUDA, T. 1972 A temperature adjustment process in a Boussinesq fluid via a buoyancy-induced meridional circulation. *J. Fluid Mech.* **54**, 417–421.

SCHLADOW, S. G., PATTERSON, J. & STREET, R. L. 1989 Transient flow in a side-heated cavity at high Rayleigh number: a numerical study. *J. Fluid Mech.* **200**, 121–148.

SCHLICHTING, H. 1968 *Boundary Layer Theory.* McGraw-Hill.

VASSEUR, P. & ROBILLARD, L. 1982 Natural convection in a rectangular cavity with wall temperature decreasing at a uniform rate. *Warme-u. Stoffubertr.* **16**, 199–207.

XIA, Q., YANG, K. T. & MUKUTMONI, D. 1995 Effect of imposed wall temperature oscillations on the stability of natural convection in a square enclosure. *Trans. ASME* C: *J. Heat Transfer* **117**, 113–120.

YEWELL, R., POULIKAKOS, D. & BEJAN, A. 1982 Transient natural convection experiments in shallow enclosures. *Trans. ASME* C: *J. Heat Transfer* **104**, 533–538.